Forming of a Very Unbalanced Fabric Experiment and Simulation

Jean-Luc L Daniel, Damien Soulat, François Dumont, Bassem Zouari, Philippe Boisse

Forming of a very unbalanced fabric. Experiment and simulation.

J.L. Daniel*— D. Soulat*— F. Dumont*— B. Zouari*— P. Boisse*— A.C. Long**

** LMSP UMR CNRS 8106 ENSAM-ESEM,*
ENSAM, 151 Bd de l'Hôpital 75013 Paris
ESEM, 8 rue Léonard de Vinci, 45072 Orléans, France
Philippe.Boisse@univ-orleans.fr

*** School of Mechanical, Materials, Manufacturing Engineering & Management,*
University of Nottingham, University Park, Nottingham NG7 2RD, UK
Andrew.Long@nottingham.ac.uk

ABSTRACT: The deep drawing of a very unbalanced fabric on a hemispherical shape is performed both experimentally and by a numerical simulation. The shape obtained depends mainly on the mechanical behaviour of the fabric and is highly non-symmetric. The simulation of the forming process is performed using finite elements based on the tensile energy of each yarn. This approach leads to very simple expression of the interior load vectors used in the explicit dynamic approach. The result of the simulation correctly describes the shape after forming and its non-symmetry. Such a result could not have been obtained by a fishnet method classically used for fabric draping.

KEY WORDS: Experimental fabric forming. Finite element simulations, Unbalanced fabric, Fabric mechanical behaviour.

1 Introduction

The use of fibre fabrics as reinforcements for composite materials is increasing because it gives the possibility to obtain complex shapes in a single operation, for a lighter final product. For instance the R.T.M. process consists of a drawing operation of the fabric before a thermoset resin is injected [CAR 96][BIC 97] [LON 98][POT 99]. The forming modes of fabrics are specific to this material and related to its woven constitution. A simulation code permits to answer two questions at the conception stage: Firstly, is the requested shape reachable by forming the fibre fabric? Secondly, where are the reinforcement directions after forming? Several codes based on geometrical approaches have been developed [MAC 56] [VAN 91][LON 94][BIC 97][WAN 99]. These methods, called fishnet algorithms, are very fast and efficient especially for the simulation of hand operated draping. Nevertheless in the case of forming with punch and die the static boundary conditions may be very important. So is the influence of the loads on the blank holder. In addition the specifications of the fabric, i.e. the material for the warp and the weft, their respective size or the way it is woven, should be included in the analysis. An objective of this paper is to show that the mechanical properties of the fabric can be very important for the result of the shaping process. The mechanical behaviour of dry fabrics such as used in the forming stage of the R.T.M. process depends on the yarn behaviour and on the weave pattern, leading to interactions between warp and weft directions and non-linear behaviour. These geometrical non-linearities due to changes in yarn crimp under tension have been studied from biaxial tests on cross-shaped specimens [BUE 01][BOI 01b]. The fabric studied in the present paper is very unbalanced. The rigidity in warp direction is much larger than in the weft direction.

An experimental forming test is presented that shows the very large effect of the non-symmetry of the fabric behaviour on the forming result. This forming process is simulated, within an explicit dynamic approach, using simplified finite elements in which the interior load vectors are calculated from the tensile energy of each yarn. This approach gives a computed fabric shape after forming in good agreement with the experimental result. The test performed experimentally and simulated clearly shows that it is necessary in this case to use a method that accounts for the fabric mechanical behaviour (and for the boundary condition) to obtain a good simulation result.

2. Deep drawing tests

2.1. *Punch and die geometry*

The tests were performed in the composites laboratory of the School of MMMEM at the University of Nottingham [RUD 99]. Cold press mouldings were held with a hemispherical punch-die couple, mounted on a classical 25kN-Instron machine (Figure 1).

A 6 kg ring was used as a blank-holder, to avoid premature wrinkles in the reinforcement. The preforms were impregnated with a translucent polyester resin after forming to freeze their movements. A grid of 10mmx10mm elements was drawn on the fabric prior to forming to measure the fibre angle variations and the elongations in each direction. The tool geometry (including the blank-holder) is shown in Figure 2.

Figure 1. *Punch-die couple*

2.2. *Very unbalanced fabric*

The fabric studied here is a 2x2 nylon twill, used in automotive parts as a reinforcement in elastomer composites. Each tow contains approximately 40 fibres. The peculiarity of this reinforcement lays in the weft tows. They are textured, so that they have a double crimped path: the normal weaving crimp and their own waviness due to their texturizing (Figure 3).

This strong difference between warp and weft tows results in a very unbalanced mechanical behaviour, as shown in Figure 4. Uni-axial traction tests exhibit a non-linear behaviour. But, for a given range of elongation, it is possible to define an

equivalent linear modulus in each direction (given in Table 1).

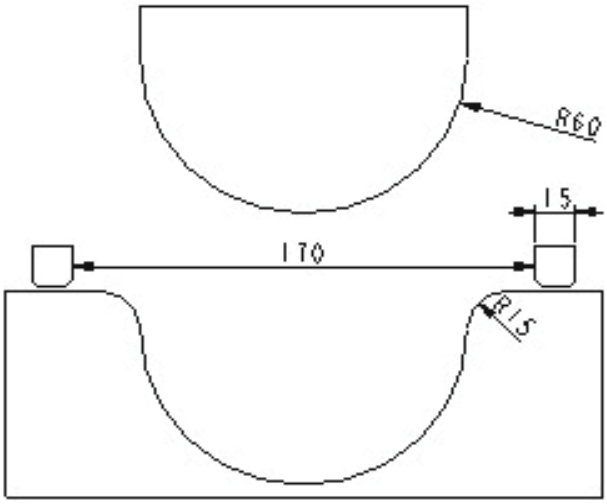

Figure 2. *Tool geometry*

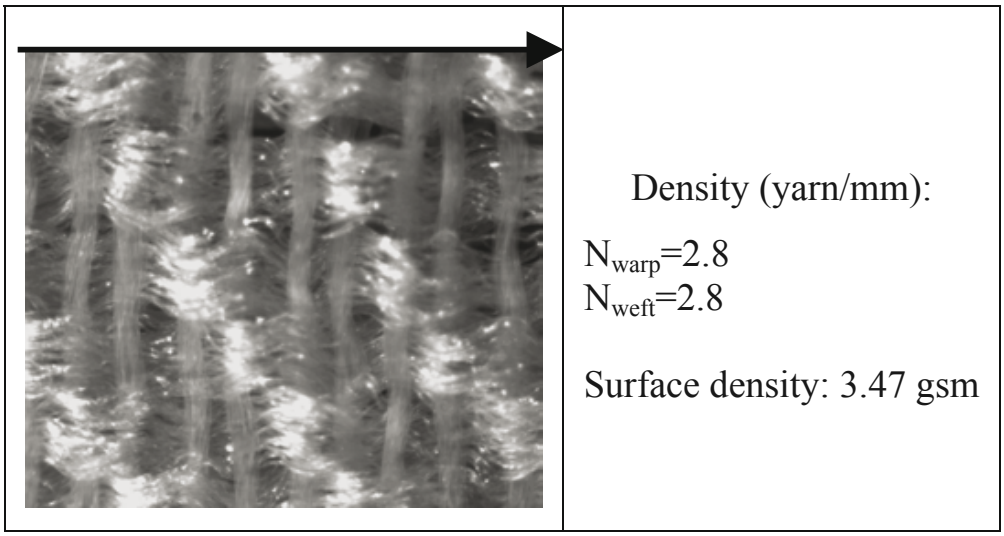

Figure 3. *Weaving characteristics of the unbalanced fabric*

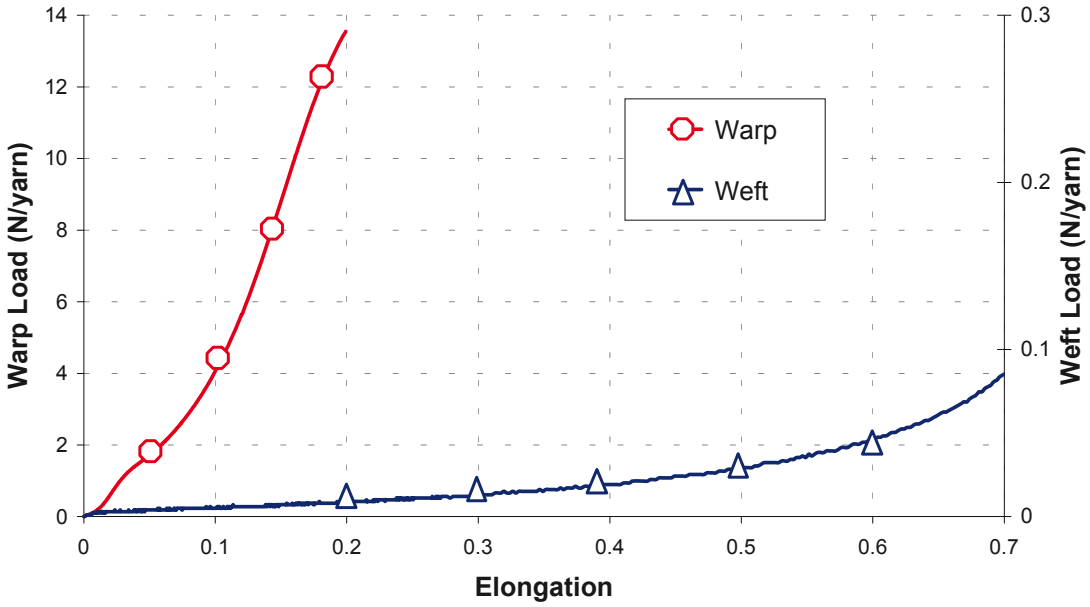

Figure 4. Warp and weft tensile behaviour

E_{Warp} (N/yarn) (until fibre fracture)	E_{Weft} (N/yarn) (0 < Elongation < 0.85)	E_{warp}/E_{weft}
50	0.2	250

Table 1. *Equivalent modulus.*

2.3. *Forming experiment*

The size of the initially square elements of the grid changes when forming. The elongation ratio between warp and weft direction can be measured easily along a line of elements (Figure 5a). At the top of the hemisphere, the weft elongation is maximum, and the warp elongation remains very low. Thus, the ratio reaches 1/1.8, which is very specific to this unbalanced fabric. In the meantime, warp and weft deformed edges of the blank (Figure 5b) exhibit strong differences. The shear angle has been measured on one quadrant (Figure 5b) by an optical method in use at the University of Nottingham. The deformed grid (Figure 6) exhibits a highest shear angle of 39°, at the base of the hemisphere. It is not symmetrical, this angle is maximum at the approximate meridian direction $\Phi = 30°$, from the warp direction (so-called 0° direction). On a balanced fabric, due to the symmetry, the maximum shear angle direction is located at $\Phi = 45°$ [AUB 89][RUD 99][YE 97].

3. Simulation of the forming process

3.1. *Simplified dynamic equation*

Fabrics are made of fibres assembled in yarns which are woven. This internal structure permits some motions between the fibres. Consequently most stiffnesses are very weak in comparison to tensile stiffness. Of course, if these possible motions (or nil rigidities) are an advantage during the forming stage they are not acceptable in the service life of the part, and it is one of the main roles of the resin that is injected after the preforming of the fabric to avoid the relative motion of the fibres. However in the forming stage the fabric is "dry" and the stress state can be assumed to be in the form :

$$\sigma = \sigma^{11}\ \mathbf{h}_1 \otimes \mathbf{h}_1 + \sigma^{22}\ \mathbf{h}_2 \otimes \mathbf{h}_2 \qquad [1]$$

σ is the Cauchy stress tensor and $\mathbf{h}_1$ and $\mathbf{h}_2$ are unit vectors in the current warp and weft directions. Defining the tension tensor by

$$\mathbf{T} = T^{11}\ \mathbf{h}_1 \otimes \mathbf{h}_1 + T^{22}\ \mathbf{h}_2 \otimes \mathbf{h}_2 \qquad [2]$$

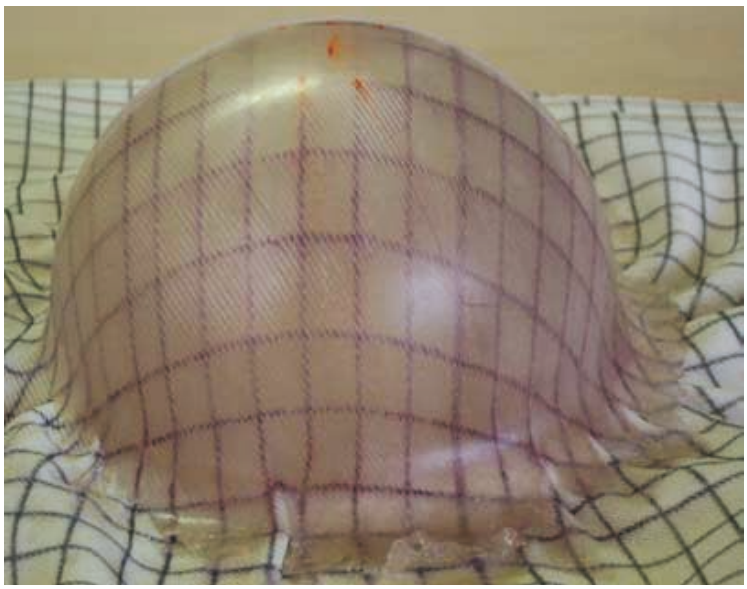

(a)

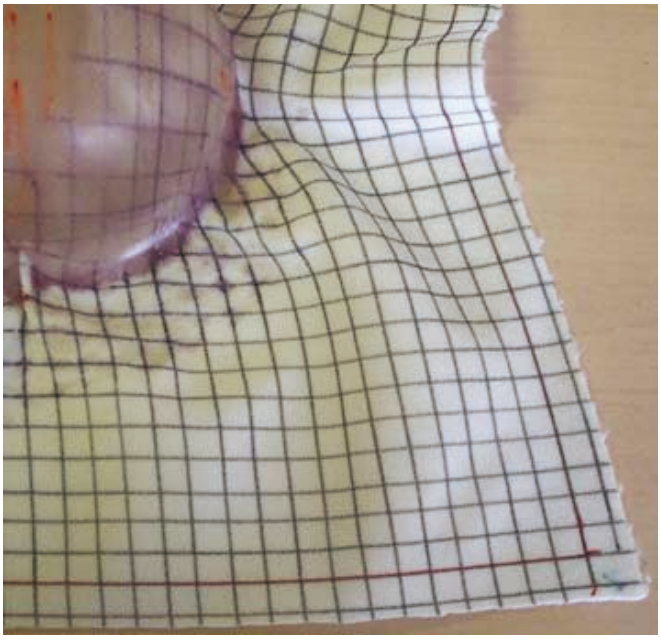

(b)

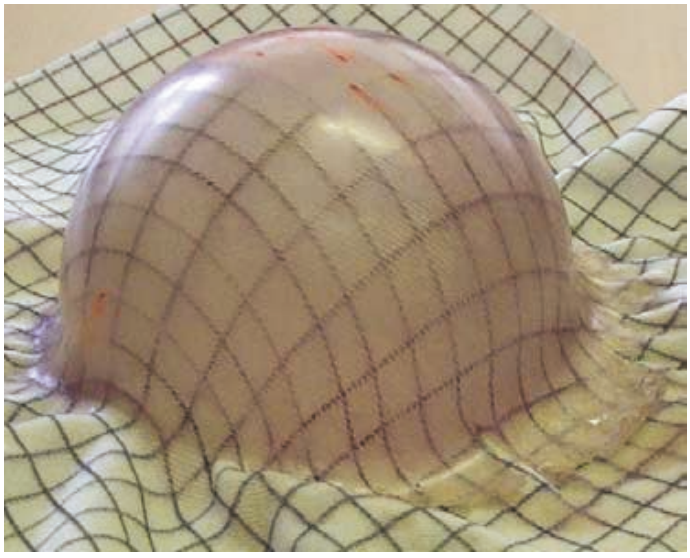

(c)

Figure 5. *Shape of the unbalanced fabric after forming*

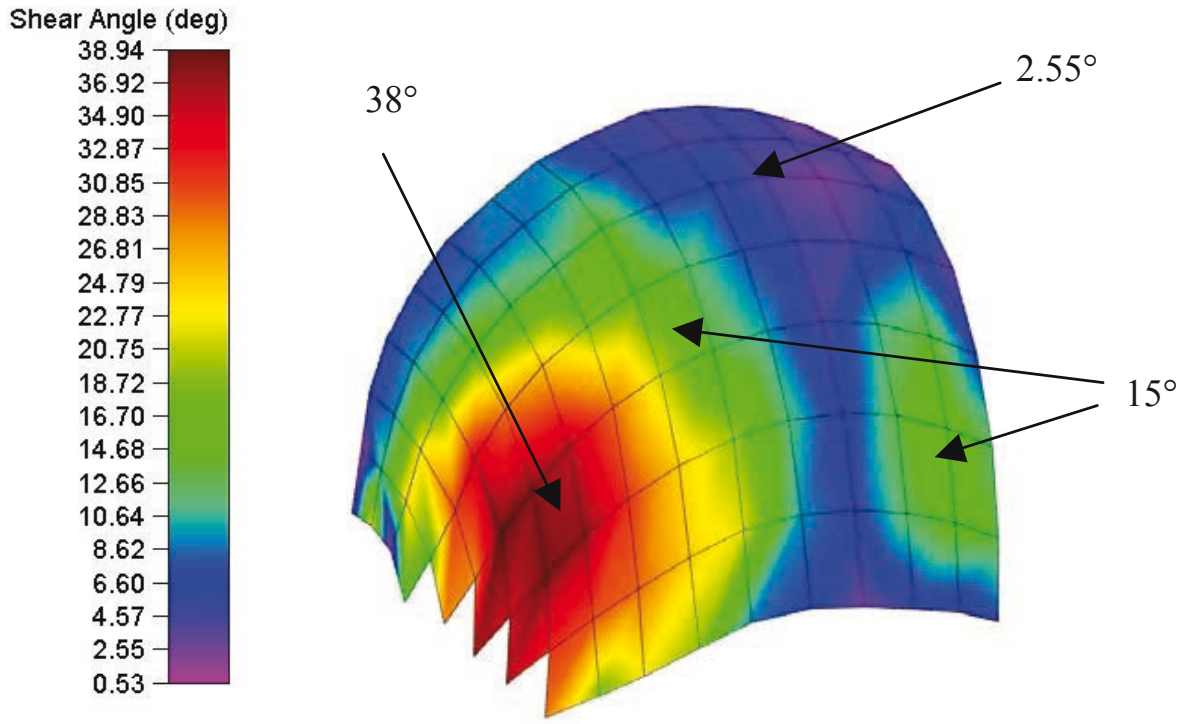

Figure 6. *Shear angle map on a quarter hemisphere measured by optical method*

with:

$$T^{11} = \int_{A_1} \sigma^{11}\, dS \quad , \; T^{22} = \int_{A_2} \sigma^{22}\, dS \quad , \; T^{11} \geq 0 \; , T^{22} \geq 0 \qquad [3]$$

For a woven domain made of ncell elementary woven cells, the dynamic equation can be written in the following simplified form [BOI 01b] :

$$\sum_{p=1}^{ncell} {}^{p}\varepsilon_{11}(\eta)\; {}^{p}T^{11}\; {}^{p}L_1 \; + \; {}^{p}\varepsilon_{22}(\eta)\; {}^{p}T^{22}\; {}^{p}L_2 \; - T_{ext}(\eta) = \int_{\Omega} \rho \overset{\circ\circ}{\mathbf{u}}.\eta \, dV \qquad [4]$$

$$\forall\, \eta \,/\, \eta = 0 \;\text{ on }\; \Gamma_u$$

$\boldsymbol{\eta}$ is the virtual displacement field with η=0 on the part of the boundary of Ω with prescribed displacements Γ_u. L_α (α=1 or 2) is the current length of the elementary cell in direction α. $\varepsilon = \varepsilon_{\alpha\beta}\, \mathbf{h}^{\alpha} \otimes \mathbf{h}^{\beta}$ is the symmetrical gradient strain tensor. $\mathbf{u}$, $\overset{\circ}{\mathbf{u}}$, $\overset{\circ\circ}{\mathbf{u}}$ are the displacement, speed and acceleration vectors and ρ is the mass per unit volume. $T_{ext}(\eta)$ is the virtual work of the exterior loads:

$$T_{ext}(\eta) = \int_{\Omega} \mathbf{f}.\eta \, dV - \int_{\Gamma t} \mathbf{t}.\eta \, dS \qquad [5]$$

f and **t** are exterior prescribed volume and surface loads.

3.2. *Explicit finite element analysis*

The simplified dynamic equation [4] is used in an explicit dynamic finite element approach. (An implicit quasi static approach can be found in [BOI 97]). If the domain Ω is divided in finite elements, the dynamic equation can be written as :

$$\mathbf{M}\ddot{\mathbf{u}}_n = \mathbf{F}_{ext} - \mathbf{F}_{int} \qquad [6]$$

M is the mass matrix, $\mathbf{F}_{ext}$ and $\mathbf{F}_{int}$ are exterior and interior nodal loads. Subscript n refers to nodal quantities and superscript e refers to an element. In the central difference scheme the solution $\mathbf{u}_n^{i+1}$ on a time step Δt^i, from t^i to t^{i+1} is calculated from $\mathbf{u}_n^i$ by :

$$\mathbf{u}_n^{i+1} = \mathbf{u}_n^i + \left(\dot{\mathbf{u}}_n^{i-1/2} + \frac{1}{2}\left(\Delta t^{i-1} + \Delta t^i\right) \mathbf{M}_D^{-1}\left(\mathbf{F}_{ext}^i - \mathbf{F}_{int}^i \right) \right) \Delta t^i \qquad [7]$$

$\mathbf{M}_D$ is a diagonal matrix calculated from the mass matrix [ZIE 89]. The numerical scheme [7] is stable only if the time step is small enough [BEL 83a]. From the simplified dynamic equation [4], a particular form is obtained for equation [6] where the virtual interior work (and consequently the internal loads) is in the form :

$$T_{int}(\boldsymbol{\eta}) = \sum_{elt} \sum_{p=1}^{n\,cell^e} \left(\eta_n^e\right)^T \mathbf{F}_{int}^e = \sum_{elt} \sum_{p=1}^{n\,cell^e} {}^p\varepsilon_{11}(\eta)\ {}^pT^{11}\,{}^pL_1 + {}^p\varepsilon_{22}(\eta)\ {}^pT^{22}\,{}^pL_2 \qquad [8]$$

with $\mathbf{F}_{int} = \underset{elt}{A}\mathbf{F}_{int}^e$ where $\underset{elt}{A}$ is the assembling operator over the elements.

The finite element briefly described below is based on the computation of the interior loads given by equation [8] with a bilinear interpolation scheme.

3.3. *Interior loads of a bilinear element*

The four node element presented Figure 7 is composed of woven yarns. The numbers of yarns in the warp and weft directions are N_c and N_t.

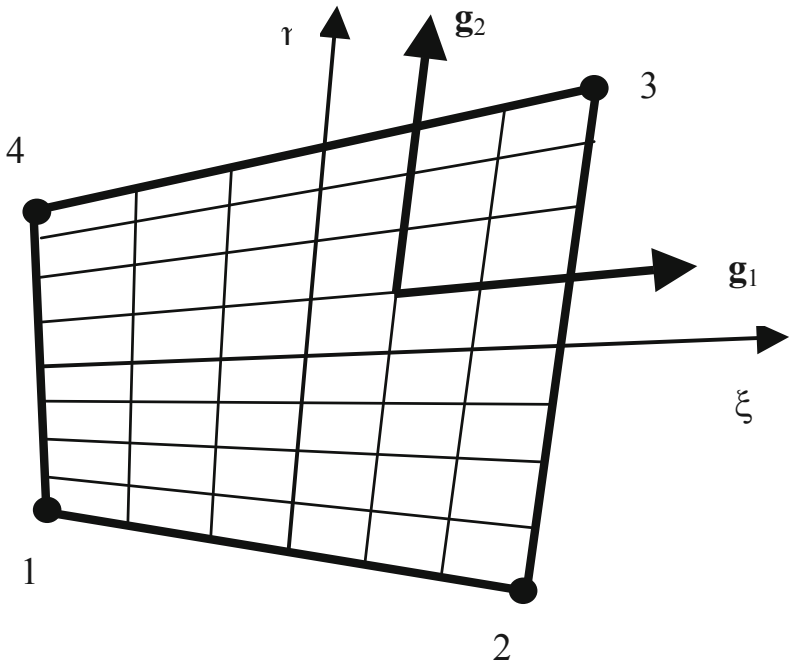

Figure 7. Bilinear fabric element

From the natural coordinates ξ and η, the following vectors are defined :

$$\mathbf{g}_\alpha = \frac{\partial \mathbf{x}}{\partial \xi_\alpha} \qquad \mathbf{h}_\alpha = \frac{\mathbf{g}_\alpha}{\|\mathbf{g}_\alpha\|} \qquad \mathbf{g}_\alpha . \mathbf{g}^\beta = \delta_\alpha{}^\beta \qquad \mathbf{h}_\alpha . \mathbf{h}^\beta = \delta_\alpha{}^\beta \qquad [9]$$

In the present element the interactions between warp and weft yarns are not taken into account. This is justified for the fabric presented in section 2.2. because the warp yarns are very much stiffer than the weft yarns. For other fabrics the effect of the weaving and the interaction between warp and weft yarns can be important. In this case the tensile behaviour must be obtained by biaxial tensile tests [BUE 01] [BOI 01b]. Finite elements including the interaction due to weaving have been developed in [BOI 97][BOI 01a]. Let us consider firstly the yarns in direction $\mathbf{g}_1$. For one element, the interior virtual work can be written as:

$$T^e_{int}(\boldsymbol{\eta}) = \sum_{yarns} \int_1 \varepsilon_{11} T^{11} ds \qquad [10]$$

The components of the gradient tensor are considered in $\mathbf{h}^1$, $\mathbf{h}^2$ and $\mathbf{g}^1$, $\mathbf{g}^2$ bases:

$$\nabla^s \boldsymbol{\eta} = \varepsilon_{\alpha\beta} \mathbf{h}^\alpha \otimes \mathbf{h}^\beta = \overline{\varepsilon}_{\alpha\beta} \mathbf{g}^\alpha \otimes \mathbf{g}^\beta \qquad [11]$$

The component of the gradient $\overline{\varepsilon}_{11}$ is related to the interpolation functions :

$$\overline{\varepsilon}_{11} = \frac{\partial \boldsymbol{\eta}}{\partial \xi} . \mathbf{g}_1 = \frac{\partial N^k}{\partial \xi} \eta_k . \mathbf{g}_1 = B_{11s} \eta_s \qquad [12]$$

The virtual interior work can be written as

$$T^e{}_{int}(\boldsymbol{\eta}) = \eta_s \sum_{yarns} \int_1 \frac{1}{\|\mathbf{g}_1\|^2} B_{11s} T^{11} ds = \eta_s (F^e_{int})_s \qquad [13]$$

The quantities present in the interior loads do not depend of ξ. Taking into account that

$$ds = \|\mathbf{g}_1\| d\xi \qquad [14]$$

the interior loads for both warp and weft yarns are :

$$(F^e_{int})_s = \sum_{\text{Warp yarns}} \frac{1}{\|\mathbf{g}_1\|} B_{11s} T^{11} + \sum_{\text{Weft yarns}} \frac{1}{\|\mathbf{g}_2\|} B_{22s} T^{22} \qquad [15]$$

Because of the bilinear interpolation function of the element, it is not necessary in the previous equation to sum over all the yarns. [15] is equivalent to :

$$(F^e_{int})_s = \sum_{p=1}^{2} N_C B_{11s} T^{11} \frac{1}{\|\mathbf{g}_1\|} + \sum_{p=1}^{2} N_T B_{22s} T^{22} \frac{1}{\|\mathbf{g}_2\|} \qquad [16]$$

N_C and N_T are the number of yarns in warp and weft directions respectively. The quantities B_{11s}, T^{11}, $\mathbf{g}_1$ (and similarly B_{22s}, T^{22}, $\mathbf{g}_2$) are evaluated at position $-\xi_p$ for p=1 and ξ_p for p=2, (and similarly for η_p) with

$$\xi_p = \sqrt{\frac{1}{3}\frac{N_c^{\,2}-1}{N_c^{\,2}}} \qquad \eta_p = \sqrt{\frac{1}{3}\frac{N_t^{\,2}-1}{N_t^{\,2}}} \qquad [17]$$

The interior loads components are given explicitly as the sum of four scalars. Consequently the element is numerically efficient. Within a dynamic explicit approach such as described in section 3.2. it is classical to use reduced integration. In that case the terms of equation [16] are only computed at the center of the element. Such an approach must avoid the zero energy mode by using a specific method [BEL 83b]. This element is included in the PAM FORM code [DEL 98].

4. Simulation of the forming of a very unbalanced fabric

The experimental forming operation described in section 2 is simulated using the four node fabric element described in section 3. The initial mesh used for the fabric, the punch, the die and the blank-holder are shown in Figure 8.

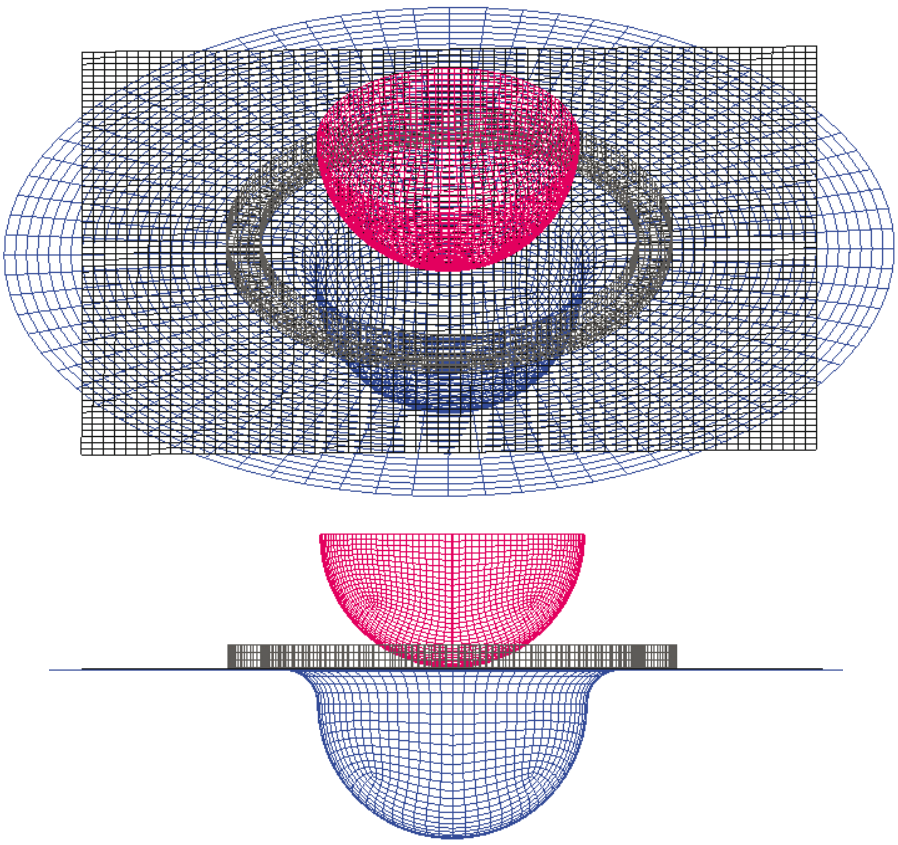

Figure 8. *Initial mesh of the fabric, the punch, the die and the blank-holder*

The deformed shape obtained at the end of the punch displacement is shown in Figure 9 and compared to the experimental shape. The global shape is correctly described by the computation. The main feature of this deformed shape is that it is very different in the warp and weft directions. The weft direction is the weak direction and it is horizontal on Figure 9. The stretching in this direction is very large in the central part due to the blank holder. The displacements of points on the edge and on the horizontal axis are very small. On the contrary the stretching in the warp (vertical) direction is small and consequently the points on the edge and on the vertical axis exhibit large displacements towards the centre of the hemisphere.

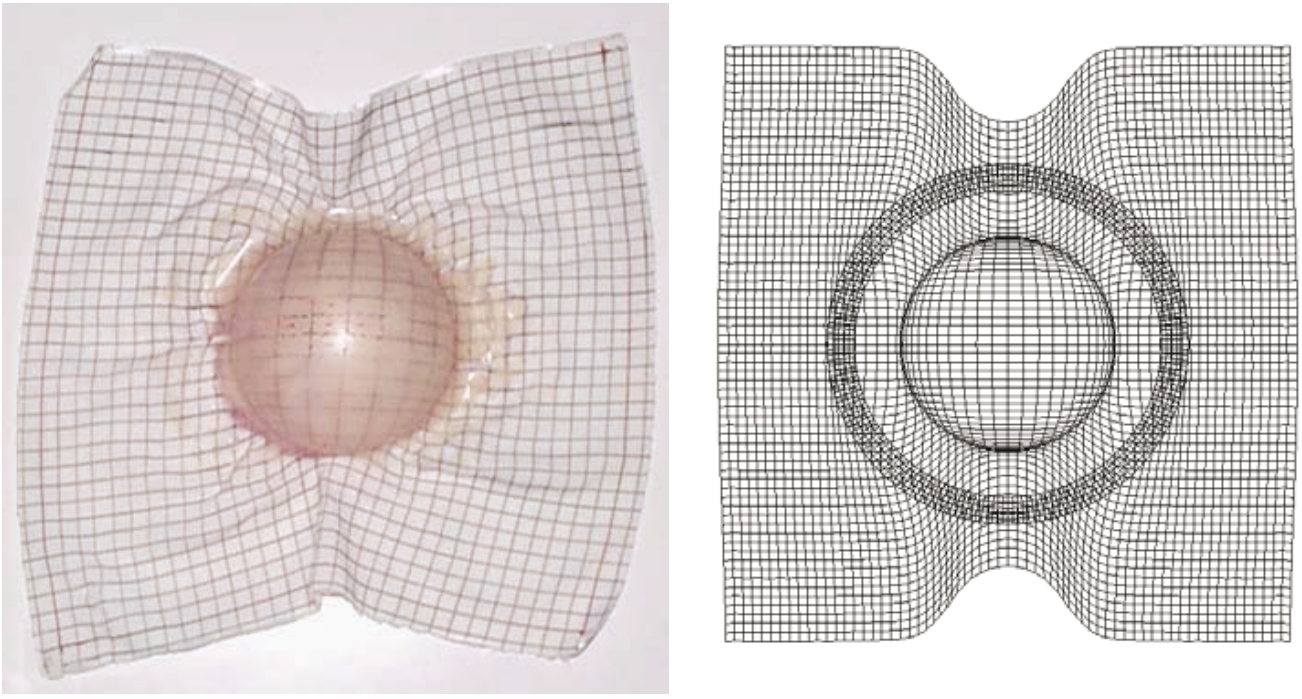

Figure 9. *Deformed shape. Comparison between experiment (left) and computation (right).*

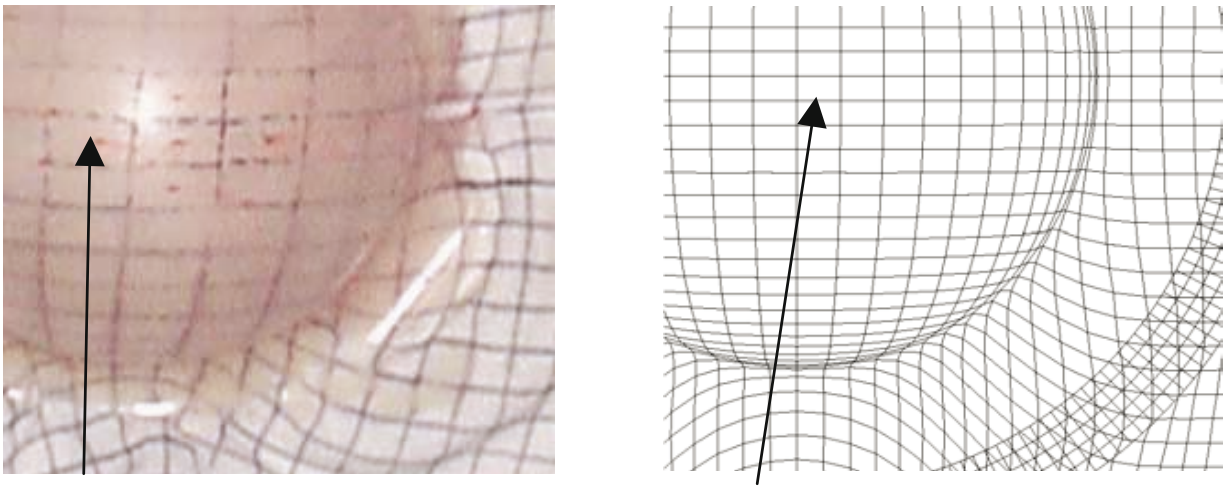

Lweft/Lwarp = 1.8

Lweft/Lwarp = 1.87

Figure 10. *Warp and weft deformations at the top of the hemisphere. Experiment (left) and computation (right).*

The computed deformed shape does not contain any wrinkles. This is due to the lack of instability in the solutions obtained from the present formulation that only considers tensile deformation energy. Taking into account the in-plane shear stiffness, especially after the limit angle would be a source of wrinkles. Some works are now in progress at LMSP in that goal. To correctly describe the wrinkle shape, it is also necessary to add some bending stiffness of the fabric in the formulation. Nevertheless many of the wrinkles in the flat part are due to removal of the blankholder and there are no wrinkles in the hemispherical part. In this region, the global shape and the in plane strain of the fabric after forming are correctly simulated by the above presented element.

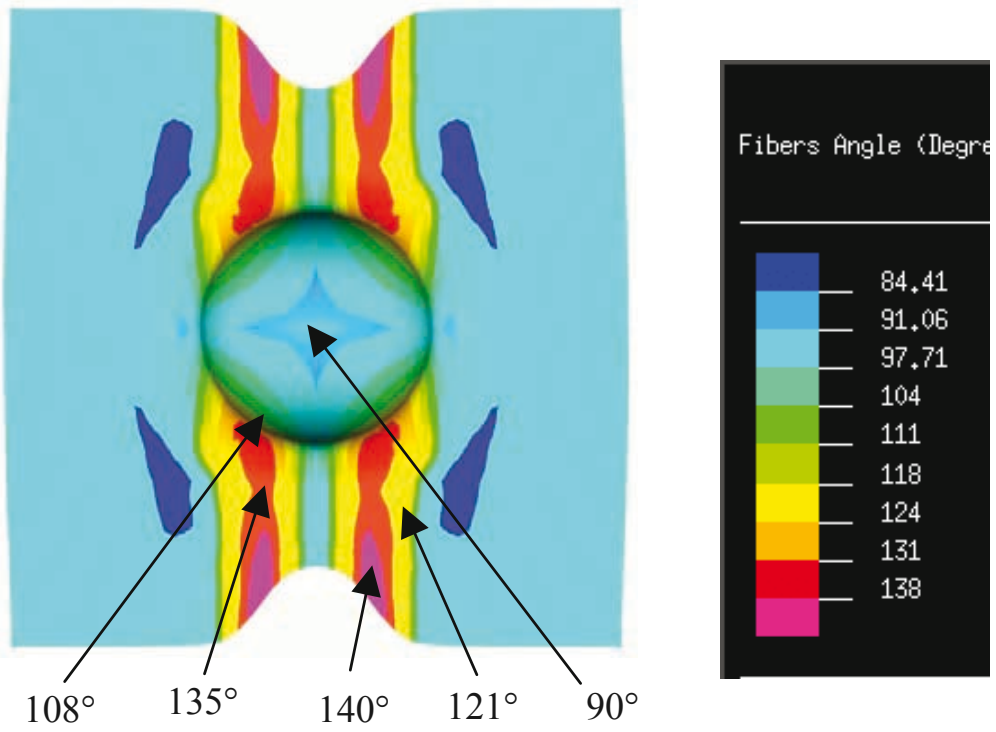

Figure 11. *Angles between warp and weft yarns after forming*

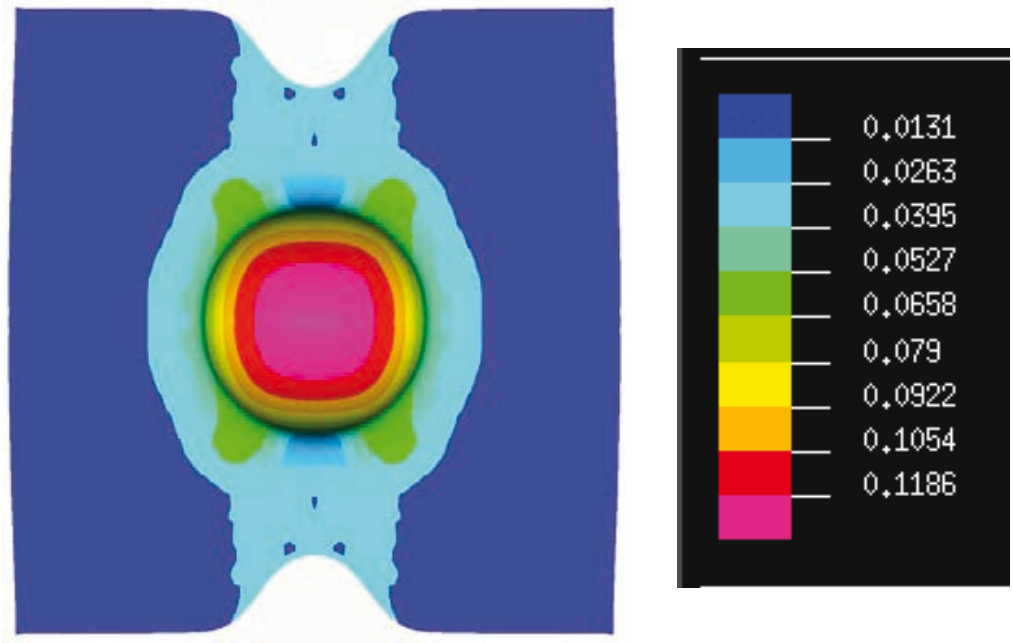

Figure 12. *Tensions in the weft direction (N/yarn)*

In the hemispherical part, the initial squares drawn on the fabric are strongly deformed and become rectangular. At the top of the hemisphere the ratio of the side length in weft and warp directions is 1.8 (Figure 10). The simulation is in good agreement with this value and gives 1.87 for this ratio. If this forming process is simulated using a classical geometrical approach (fishnet algorithm) this ratio would be equal to 1 and the computed shape would be symmetrical which is very far from the experimental results.

Figure 11 shows the in plane shear deformation i.e. the angles between warp and weft yarns after forming. The position of the high shear zone is in correct agreement with the experiment even if the wrinkles in the experimental part modify the value of the shear angle. The angles between warp and weft yarns are not symmetrical and depend mainly on the imbalance of the fabric.

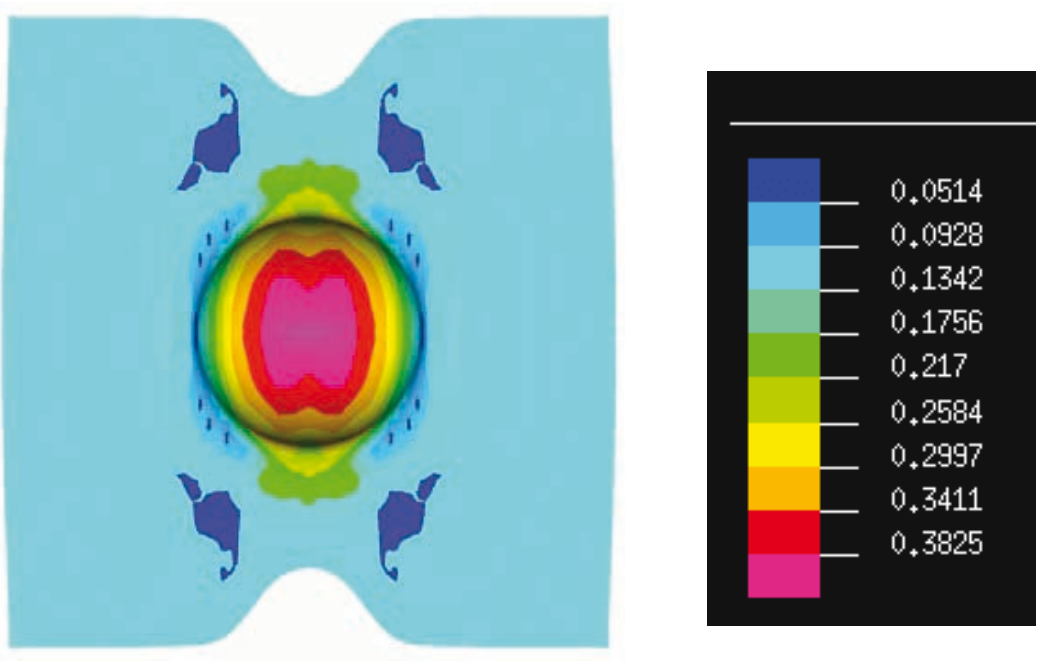

Figure 13. *Tensions in the warp direction (N/yarn)*

Finally Figures 12 and 13 give the tensions in the warp and weft directions. The computation of these tensions is an important advantage of finite element approach. For instance the maximal possible load on the blank holder can be determined by these yarn tensions. The computed tensions and tensile strains are large in the hemispherical part especially for the weft yarns which are not very far from the ultimate value. The tensile strain is 0.87 while the tensile strain at failure is 1.1.

5. Conclusions

An hemispherical forming experiment performed on a very unbalanced fabric has shown that the result is highly non-symmetric. This result cannot be obtained by classical geometric draping algorithms. A simplified finite element based on the

tension energy of each yarn has been used with an explicit dynamic approach. The computed shape after forming is in correct agreement with the experimental one. The wrinkles are not modelled at present. With this in mind elements with in plane shear and bending stiffness are now being developed.

This example clearly shows that the mechanical behaviour of the fabric can be important in a forming process. In this case a mechanical approach is necessary to account for this aspect. The static boundary conditions i.e. the loads on the tools can also be very important for the final result of forming. Their modelling also needs a finite element approach.

6. Acknowledgement

This work was performed with the support from PSA, EADS and ESI companies. This support is gratefully acknowledged by the authors.

7. References

[AUB 89] Aubourg, N. Mion, D., Etude de la Modélisation de l'emboutissage d'un tissu de fibres de verre. *Report PSA/Ecole Polytechniqu*e, 1989 (in french)

[BEL 83a] Belytschko, T., An overview of semidiscretisation and time integration procedures, Computation methods for transient analysis, ed. T. Belytschko & T.J.R.Hughes, Elsevier Science, 1983, 1-65

[BEL 83b] Belytschko T., Tsay C.S., A stabilization procedure for the quadrilateral plate element with one point quadrature, *International Journal for Numerical Methods in Engineering*, Vol. 19, p275-290, 1983.

[BIC 97] Bickerton, S., Simacek, P., Guglielmi, S.E. And Advani, S.G. Investigation of draping and its effects on the mold filling process during manufacturing of a compound curved composite part. Composite Part A, 28, 1997, 801-816

[BOI 97] Boisse P., Borr M., Buet K. and Cherouat A. "Finite element simulation of textile composite forming including the biaxial fabric behaviour", *Composites B*, Vol 28B, 1997, p.453-464

[BOI 01a] Boisse P., Daniel J.L., Hivet G., Soulat D. "A simplified explicit approach for simulations of fibre fabric deformation during manufacturing preforms for R.T.M. process". *International Journal of Forming Processes*, 2001,Vol.3, n°3-4, pp.331-353.

[BOI 01b] Boisse, P., A. Gasser, and G. Hivet, Analyses of fabric behaviour : determination of the biaxial tension-strain surfaces and their use in forming simulations. *Composites Part A*. 32-10 (2001) 1395-1414

[BUE 01] Buet K., Boisse Ph., "Experimental analysis and models for biaxial mechanical behaviour of composite woven reinforcements", *Experimental Mechanics,* 41, 3,260-269, 2001

[CAR 96] Carronnier D. et Gay D., "Approche intégrée du RTM", *Revue des composites et des matériaux avancés*, 6, special issue, 1996, Hermès, (in french)

[DEL 98b] De Luca, P., Pickett, A.K.,Industrial examples of forming non-metallic parts using PAM-FORM^{TM}, Proceedings of PAM'98, PSI/ESI Group, Tours, France, 1998, 1-18.

[LON 94] Long, A.C. and Rudd C.D., A simulation of reinforcement deformation during the production of preforms for liquid moulding processes. I. Mech. E. J. Eng. Manuf., 208, 1994, 269-278
[LON 98]Long A.C., Blanchard P.J., Rudd C.D., Smith P. The development of an integrated process model for liquid composite moulding, Composites Part A, 1998, 29A, 847-854
[MAC 56] Mack, C. nnd Taylor H. M. The fitting of woven cloth to surfaces. Journal of Textile Institute, 1956, Vol. 47, pp. 477-488
[POT 99] Potter K.D. The early history of the resin transfer moulding process for aerospace applications, Composites Part A, 1999, 30 (5), 619-621
[RUD 99] Rudd, C.D., M.R. Turner, A.C. Long, and V. Middleton, Tow placement studies for liquid composite moulding. *Composites Part A*.. 30-9 (1999) 1105-1121
[VAN 91] Van Der Ween, F., "Algorithms for draping fabrics on doubly curved surfaces", *International Journal of Numerical Method in Engineering*, Vol. 31, 1991, p. 1414-1426
[WAN 99] Wang, J., Paton, R., Paye, J.R.,The draping of woven fabric preforms and prepregs for production of polymer composite components, Composites A, 30, 1999, 757-765
[YE 97] Ye, L. and H.R. Daghyani, Characteristics of woven fibre fabric reinforced composites in forming process. *Composites Part A*. 28A (1997) 869-874.
[ZIE 89] Zienkiewicz O. and Taylor R., The finite element method, 1, McGrawHill, 1989